

Electrochemistry at Edge of Single Graphene Layer in a Nanopore

Shouvik Banerjee, Jiwook Shim, Jose Rivera, Xiaozhong Jin, David Estrada, Vita Solovyeva, Xiuque You, James Pak, Eric Pop, Narayana Aluru, and Rashid Bashir

ACS Nano, **Just Accepted Manuscript** • DOI: 10.1021/nn305400n • Publication Date (Web): 18 Dec 2012

Downloaded from <http://pubs.acs.org> on December 20, 2012

Just Accepted

“Just Accepted” manuscripts have been peer-reviewed and accepted for publication. They are posted online prior to technical editing, formatting for publication and author proofing. The American Chemical Society provides “Just Accepted” as a free service to the research community to expedite the dissemination of scientific material as soon as possible after acceptance. “Just Accepted” manuscripts appear in full in PDF format accompanied by an HTML abstract. “Just Accepted” manuscripts have been fully peer reviewed, but should not be considered the official version of record. They are accessible to all readers and citable by the Digital Object Identifier (DOI®). “Just Accepted” is an optional service offered to authors. Therefore, the “Just Accepted” Web site may not include all articles that will be published in the journal. After a manuscript is technically edited and formatted, it will be removed from the “Just Accepted” Web site and published as an ASAP article. Note that technical editing may introduce minor changes to the manuscript text and/or graphics which could affect content, and all legal disclaimers and ethical guidelines that apply to the journal pertain. ACS cannot be held responsible for errors or consequences arising from the use of information contained in these “Just Accepted” manuscripts.



Electrochemistry at Edge of Single Graphene Layer in a Nanopore

Shouvik Banerjee^{1,2,‡}, Jiwook Shim^{2,3,‡}, Jose Rivera^{2,4}, Xiaozhong Jin^{5,6}, David Estrada^{2,3}, Vita Solovyeva^{2,3}, Xiuque You⁷, James Pak⁷, Eric Pop^{2,3,6}, Narayana Aluru^{5,6}, Rashid Bashir^{2,3,4,★}

¹Department of Materials Science and Engineering, ²Micro and Nanotechnology Laboratory,

³Department of Electrical and Computer Engineering, ⁴Department of Bioengineering,

⁵Department of Mechanical Science and Engineering,

⁶Beckman Institute for Advanced Science and Technology,

University of Illinois at Urbana – Champaign, Urbana, IL, USA 61801

⁷School of Electrical Engineering, Korea University, Seoul, Korea

‡authors contributed equally

★ Corresponding author

rbashir@illinois.edu

1 **Abstract**

2 We study the electrochemistry of single layer graphene edges using a nanopore-based structure
3 consisting of stacked graphene and Al₂O₃ dielectric layers. Nanopores, with diameters ranging
4 from 5 to 20 nm, are formed by an electron beam sculpting process on the stacked layers. This
5 leads to unique edge structure which, along with the atomically thin nature of the embedded
6 graphene electrode, demonstrates electrochemical current densities as high as 1.2×10^4 A/cm².
7 The graphene edge embedded structure offers a unique capability to study the electrochemical
8 exchange at an individual graphene edge, isolated from the basal plane electrochemical activity.
9 We also report ionic current modulation in the nanopore by biasing the embedded graphene
10 terminal with respect to the electrodes in the fluid. The high electrochemical specific current
11 density for a graphene nanopore-based device can have many applications in sensitive chemical
12 and biological sensing, and energy storage devices.

13 **Keywords**

14 Nanopores, graphene, graphene electrochemistry, nano-bio sensors, stacked graphene

15
16 Graphene has attracted tremendous interest in the scientific world over the recent years due to its
17 unique electronic,¹⁻² thermal³ and optical⁴ properties. It has shown great promise in the field of
18 electronics, biological and chemical sensing, and energy storage applications.⁵⁻⁶ Studies on
19 graphene electrochemistry have suggested the ability of graphene based electrodes to carry a
20 large amount of current at electron transfer rates superior to graphite and carbon nanotube
21 (CNT) electrodes.⁵ The relative abundance of carbon on earth combined with widespread
22 knowledge of carbon-based chemistries and stability makes the study of graphene based
23 electrochemistry extremely exciting.^{5,7-8}

1
2
3 1 Graphene is a single atom thick sheet of sp^2 hybridized carbon atoms arranged in a honeycomb
4
5 2 lattice structure. A graphene sheet has two types of electron transfer sites – edge and basal. Edge
6
7 3 sites have already been demonstrated to possess enhanced electron transport rates and reactivity
8
9 4 in studies of CNT ends.⁹ Graphene has a higher theoretical specific surface area (2630 m²/g) than
10
11 5 graphite and CNTs (1315 m²/g) and provides motivation for study of heterogeneous electron
12
13 6 transfer rates.⁸ In addition, graphene can carry significant current densities without degradation
14
15 7 from electro-migration which typically causes significant damage in ultrathin metal films.¹⁰
16
17 8 Current densities as high as 2×10^9 A/cm² have been reported for nanoscale interconnects based
18
19 9 on graphene grown by chemical vapour deposition (CVD).¹¹ The graphene edge plane atoms
20
21 10 have been reported to have significantly higher electron transfer rate compared to basal planes in
22
23 11 electrochemical studies on both highly ordered pyrolytic graphite as well as on multiple layers of
24
25 12 graphene.¹²⁻¹³ Graphene modified glassy carbon electrodes have been reported to have much
26
27 13 greater electrochemical response, than unadulterated glassy carbon electrodes, to molecules like
28
29 14 paracetamol, hydrazine, glucose, ethanol dopamine as well as heavy metals.^{7,8} Zhou *et al.*¹⁴
30
31 15 demonstrated the ability of chemically reduced graphene oxide electrodes to distinguish the
32
33 16 electrochemical current signal from the four bases of DNA, which could not be distinguished
34
35 17 with graphite and glassy carbon electrodes. Another important application of graphene
36
37 18 electrochemistry is in energy storage devices. The specific capacitance of chemically modified
38
39 19 graphene was found to be up to 1352 F/g,⁵ and extremely high energy densities up to 85.6 Wh/kg
40
41 20 at room temperature have been reported.¹⁵⁻¹⁶ Furthermore, graphene and hybrid graphene based
42
43 21 electrodes have been used to increase specific capacities of Li⁺ ion based batteries, improving
44
45 22 power density and cyclic performance, while maintaining mechanical integrity at high current
46
47 23 densities.⁶
48
49
50
51
52
53
54
55
56
57
58
59
60

1
2
3 1 Despite extensive studies on graphene sheets and graphene doped electrodes, the electrochemical
4
5 2 properties of isolated graphene edges remain relatively unexplored. Here, we demonstrate a
6
7 3 graphene edge embedded nanopore (GEEN) structure to isolate graphene edge electrochemical
8
9 4 activity from basal plane activity. Transmission electron microscopy (TEM) based sculpting
10
11 5 offers potential for control on graphene edge structures.¹⁷ Furthermore, we demonstrate the use
12
13 6 of the embedded graphene edge to modulate the ionic flux in the nanopore. Along with a
14
15 7 conductive graphene terminal of thickness equivalent to the distance between two adjacent base
16
17 8 pairs in dsDNA (~0.34 nm), this could provide a basis for single DNA molecule analysis with
18
19 9 measurement methodologies like tunnelling or electrochemical redox reactions.
20
21
22
23

24 **Results and Discussion**

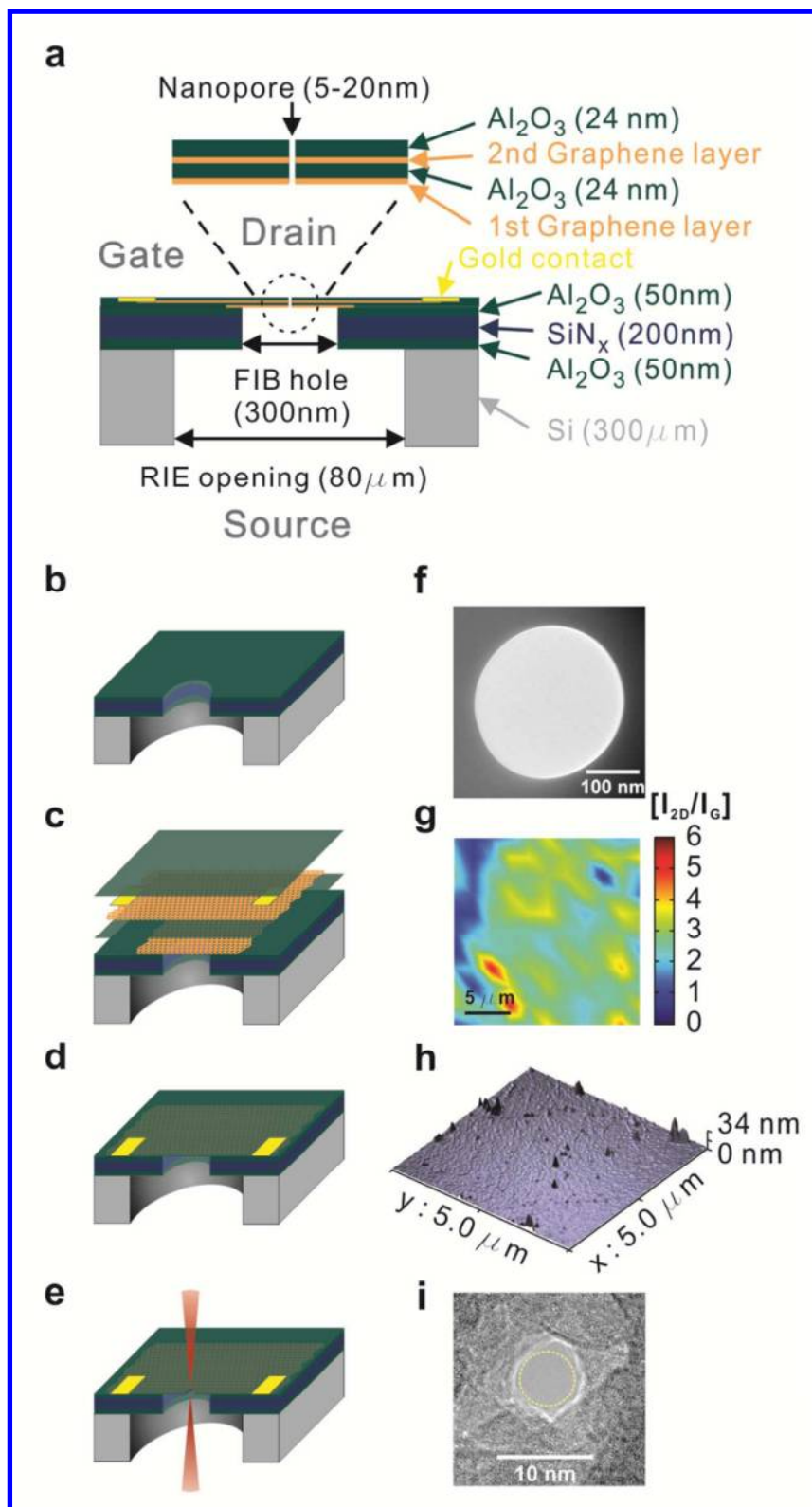
25
26
27 11 The fabrication of graphene nanopores using a TEM has been demonstrated previously and used
28
29 12 to sense biomolecules like polynucleotides and DNA protein complexes.¹⁸⁻¹⁹ In this study, we
30
31 13 fabricate GEENs in stacked graphene and dielectric layers using a focused electron beam in a
32
33 14 TEM (200 keV), and measure the electrochemical current exchange at the graphene edge
34
35 15 embedded within the nanopore. The top Al₂O₃ dielectric layer isolates the electrochemical basal
36
37 16 plane activity. We demonstrate the very high electrochemical current density as well as the first
38
39 17 known study of electrochemical current exchange at graphene (potentially as thin as single layer)
40
41 18 edge in an ionic solution. The combination of non-linear diffusion at nanoscale electrodes, an
42
43 19 enhanced concentration gradient of ions in the vicinity of the nanopore²⁰ and high electron
44
45 20 transfer rates at damaged edges of graphene¹² creates a unique system with high electrochemical
46
47 21 current densities.
48
49
50
51
52

53 22 The schematic of our test GEEN structures is shown in Fig. 1a.²¹ The fabrication process is
54
55 23 further described in Fig. 1b-e (details in the Methods section). Initially, a suspended hydrophilic
56
57
58
59
60

1 supporting membrane of stacked layers of 50 nm Al₂O₃, 200 nm SiN_x and 50 nm Al₂O₃ is
2 fabricated using deep reactive ion etching (DRIE). Subsequently, a hole of 300 ± 40 nm is
3 formed in the supporting membrane using a focused ion beam (FIB) (Fig. 1b). The graphene –
4 Al₂O₃ stack is then formed on the supporting membrane with the FIB hole by transferring
5 graphene films grown by CVD (details in the Methods section). We note that the hydrophilic
6 nature of the supporting membrane helps spread the water more evenly during the graphene
7 transfer steps and improves the smoothness of the transferred graphene/PMMA stack.²² The
8 Raman spectroscopy maps of the graphene 2D to G peak intensity ratios (I_{2D}/I_G) (Fig. 1g and
9 Supplementary Fig. 4a-b) and the full-width at half maximum of the 2D peak (FWHM_{2D})²³
10 (Supplementary Fig. 4e-f) show our growth process results in a mix of monolayer and bilayer
11 graphene, similar to our previous work.²¹ The first graphene layer (G1) in our stack spans the
12 FIB hole and acts as a mechanical support for deposition of the subsequent graphene and
13 dielectric layers of our architecture. We note that subsequent to the graphene transfers, the
14 membranes are annealed in an Ar/H₂ atmosphere at 400 °C to remove PMMA residue remnant
15 from the transfer process.²⁴

16 To ensure uniform nucleation of the subsequent Al₂O₃ deposition (D1) onto the chemically inert
17 graphene basal planes, a metallic seed layer of Al (2 nm thick) is evaporated onto the graphene.²⁵
18 Al₂O₃ is a suitable choice as the dielectric due to its excellent mechanical stability²⁶ and
19 reduction in 1/f noise compared to Si₃N₄ and SiO₂ membranes.²⁷⁻²⁸ The atomic force microscopy
20 (AFM) images (Fig. 1h and Supplementary Fig. 4d) clearly show dense and uniform deposition
21 of the dielectric due to the presence of the seed layer (Supplementary Fig. 5a-c and
22 Supplementary Fig. 7) as compared to dielectric deposition without the Al seed layer
23 (Supplementary Fig. 5a-b). ALD is chosen as it offers sub nanometer control over dielectric

1 thickness in addition to being a conformal deposition technique and a low temperature process,
2 making it compatible with the previously transferred graphene layers.²¹ The thickness of the
3 dielectric deposited is 24 nm, a value established through extensive leakage testing in fluidic
4 environments (Fig. 2 and Supplementary Fig. 1). Similar thicknesses of dielectric have been
5 reported to provide effective isolation in ionic fluid environments in transistor based devices.²⁹⁻³⁰
6 A second graphene layer (G2) is transferred onto D1 and annealed in an Ar/H₂ atmosphere. This
7 layer is contacted using Ti/Au contacts and insulated by depositing another 24 nm of Al₂O₃ (D2)
8 as described above (Details in the Methods section).



1

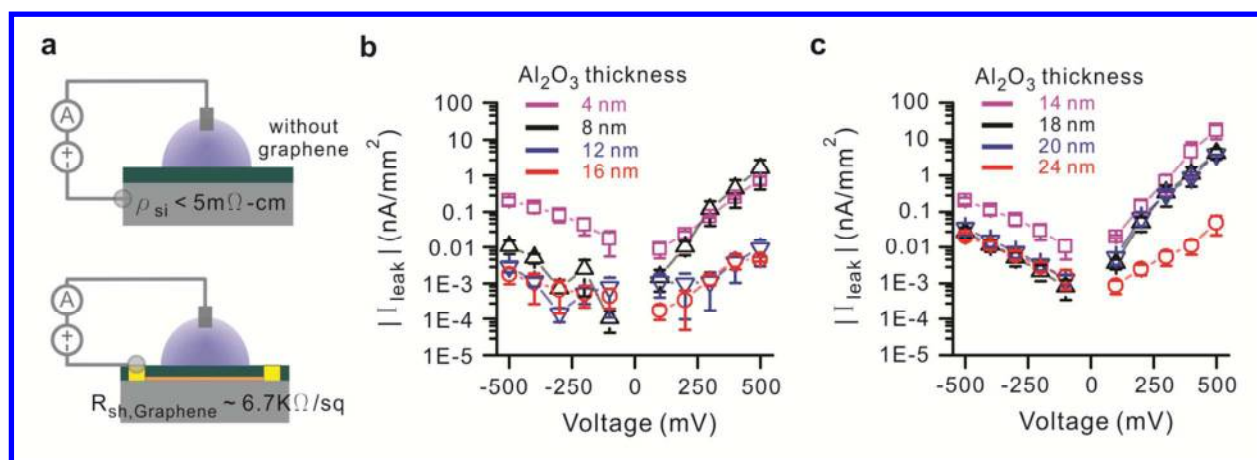
1 Figure 1. Schematic diagram of graphene-embedded stacked membrane structure and fabrication.
2 (a) Schematic showing the thickness of each layer as well as diameters of RIE, FIB and nanopore
3 holes (b) Supporting membrane consists of three layers of 50 nm of Al₂O₃, 200 nm of SiN_x and
4 50 nm of Al₂O₃, deposited on 300 μm-thick double polished prime Si wafer. RIE is used to etch
5 80 μm-wide opening in Si wafer to supporting membrane and 300 nm through hole is fabricated
6 in supporting membrane by FIB. (c) First graphene layer transferred onto the FIB hole acts as the
7 support for subsequent layers. This is insulated from the second graphene layer by 24 nm of
8 Al₂O₃ deposition. Second graphene layer, which is the active electrode at the middle of
9 membrane, is transferred onto first Al₂O₃ layer. Ti/Au deposition enables the formation of
10 contacts. A further layer of Al₂O₃ is deposited to insulate the electrode from the ionic solution.
11 (d) Final structure of graphene embedded membrane suspended on 300 nm FIB hole. (e) Focused
12 electron beam (CBED mode) in TEM is used to fabricate a single nanopore of 5 to 20 nm
13 diameter. (f) TEM image of FIB hole of 300 nm diameter in supporting membrane. (g) Raman
14 spectroscopy of I_{2D} / I_G obtained from graphene surface indicating predominantly monolayer
15 coverage. (h) AFM image of membrane surface. Roughness (Ra = 1.89 ± 0.67 nm) is
16 significantly reduced on deposition of Al₂O₃ on graphene compared to bare graphene surface (Ra
17 = 0.84 ± 0.21 nm). (i) 5nm nanopore is fabricated by convergent electron beam in TEM.

18
19 To explore the electrochemical current exchange at the graphene nanopore edges, it is essential
20 to eliminate current exchange at the basal plane from affecting our measurements. In the
21 embedded graphene membrane, the parasitic leakage current from gate to source and gate to
22 drain (indicated in Fig. 1a) could adversely affect our experimental values. The active device
23 area exposed to fluid on the backside (gate-source path) is just the area exposed to the FIB hole

1 of 300 nm. This area is insulated from the fluid by the 24 nm Al_2O_3 under the graphene gate
2 electrode. The rest of the graphene is well insulated by a total thickness of 300nm of stacked
3 Al_2O_3 and SiN_x layers of the supporting membrane structure. On the gate-drain path the entire
4 encapsulated graphene sheet is shielded from the fluid by just the top layer of 24 nm Al_2O_3 . The
5 fluid area exposed at the top layer corresponds to the area exposed by the o-rings (diameter =
6 1.42 mm) used to seal the fluidic setup. To mimic our device structure and characterize leakage
7 through the top dielectric, we fabricated the device as shown in Fig. 2 a. We compared the
8 leakage current through different thicknesses of Al_2O_3 deposited on a bare conductive silicon
9 wafer and Al_2O_3 deposited on a graphene sheet transferred onto an Al_2O_3 coated (on Si wafer)
10 top surface, similar to the D1/G2/D2 stack of our actual devices. The ALD dielectric deposition
11 of Al_2O_3 on graphene is preceded by the seed layer Al (~ 2 nm thick) evaporation as described
12 previously. The leakage is measured by attaching a PDMS well (2.75 mm in diameter) on top of
13 the device to hold the fluid. The current is measured between the graphene electrode and
14 Ag/AgCl electrode dipped in the electrolyte fluid. All leakage measurements were performed
15 with a 1 M KCl solution. The conductive silicon and the graphene electrode are connected to
16 ground in all measurements.

17 The leakage densities observed are presented on a logarithmic scale (absolute value) in Fig. 2 b-
18 c. On the bare silicon wafer, a slight asymmetry was observed in the I-V characteristics. For a
19 positive Ag/AgCl electrode voltage a higher leakage current density was observed through the
20 dielectric. The leakage current density reduces from -0.2 to -0.001 nA/mm^2 at -500 mV, as the
21 dielectric thickness is increased from 4 to 16 nm. Comparing these values to leakage currents on
22 samples with the dielectric deposited on graphene we can see a significant increase in the
23 leakage current of the latter (Fig. 2c). The electrochemical exchange at the dielectric-electrolyte

1 interface has been reported in electrolyte-oxide-silicon (EOS) devices.³¹ Since the leakage
2 current is high at positive electrode voltages, this could indicate electron tunnelling through the
3 pinholes in the dielectric as shown in our AFM images (Supplementary Fig. 4d and
4 Supplementary Fig. 9), similar to those reported in TiO₂ coated CVD graphene membranes.¹⁸ On
5 the other hand, at negative electrode voltages the leakage currents are significantly suppressed in
6 the voltage range from 0 to -500 mV. Increasing the dielectric thickness from 14 to 24 nm
7 decreases the leakage current density from -0.2 to -0.02 nA/mm². For a 2.75 mm diameter PDMS
8 well, that translates to a current of about 118.7 pA. Since the ionic current through the nanopore
9 is usually in the range of nanoamperes, at least one order of magnitude lower leakage current is
10 essential to maintain reliability of our electrochemical current measurements and to have gate
11 current independent from interference due to leakages. Therefore, we use only the negative
12 voltage range (0 to -500 mV) in our nanopore measurements to minimize and avoid leakage
13 across D2.



14
15 Figure 2. Leakage test on various thickness of Al₂O₃. (a-top) Schematics showing leakage
16 measurement setup for Al₂O₃ on p++ Silicon ($\rho < 5 \text{ m}\Omega\text{-cm}$). Al₂O₃ of thickness 4 to 16 nm were
17 deposited on the conductive Si wafer. Measurements are conducted with one electrode connected

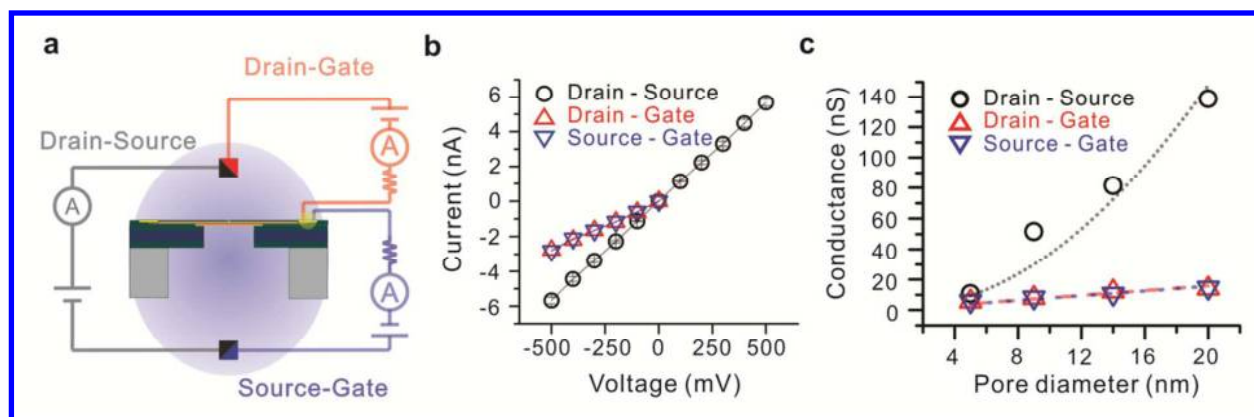
1 to Si wafer and the other attached to Ag/AgCl electrode in the solution (a-bottom) Schematic of
2 leakage measurement setup for Al₂O₃ on graphene transferred onto Si surface with Al₂O₃
3 deposited on top. Al₂O₃ thickness in range of 14 to 24 nm is deposited on graphene ($R_{sh} \approx 6.7$
4 k Ω /sq) transferred on Si wafer with a ALD deposited Al₂O₃ top surface. Measurements are
5 conducted between the graphene film contacted with aluminium wires and the solution contacted
6 with Ag/AgCl electrodes. All leakage experiments are performed in 1 M KCl, 10 mM Tris, 1
7 mM EDTA at pH 7.6 and at room temperature (22 ± 2 °C). (b) Leakage current density measured
8 for Al₂O₃ on conductive Silicon. Al₂O₃ thickness less than 10 nm showed leakage current greater
9 than 1 nA/mm² at 500 mV, but thicker Al₂O₃ (>10 nm) showed much greater insulation over the
10 voltage range of -500 mV to +500 mV. (c) Leakage current density for Al₂O₃ deposited on
11 graphene. Leakage current is observed to be fairly high up to 20 nm-thick Al₂O₃. Also the
12 leakage is significantly higher for positive voltage at Ag/AgCl electrode. 24 nm-thick Al₂O₃
13 displays decent insulation from leakage. Current leakage occurrence at relative thicker Al₂O₃
14 deposited on graphene is associated with wrinkles on graphene (Supplementary Fig. 9).

15
16 On settling upon a dielectric thickness of 24 nm, nanopores are drilled in this stacked structure
17 using convergent beam electron diffraction (CBED) mode in a TEM (Fig. 1e and 1i). We
18 fabricated four different pore diameters (5, 9, 14, 20 nm) for our test structures. For a 5nm pore,
19 the beam sputters through the membrane in about 30s. For larger pores, sculpting is needed by
20 moving the beam on the edges of the pore to expand it. Control is achieved by in-situ monitoring
21 of the nanopore dimension with imaging. Since TEM provides angstrom level precision we
22 believe the nanopore dimensions are accurate within a tolerance of 1nm. Prior to assembly in the
23 fluidic setup the backside (silicon trench side) (Fig. 1a) is O₂ plasma treated to make the pore

1 hydrophilic to facilitate wetting.^{18,21} The top graphene layer (G2) is contacted and the chip is
2 encapsulated in a custom built fluidic setup (Supplementary Fig. 6). Ethanol is then flushed into
3 both chambers to promote wetting as reported in previous nanopore studies.^{19,21} The ethanol is
4 flushed away repeatedly with de-ionized (DI) water and the desired buffer solution is inserted
5 into both chambers.

6 The schematics of drain-source, drain-gate and source-gate measurements are shown in Fig. 3a.
7 An external resistor of 20 M Ω is placed in series with graphene. This helps ensure our graphene
8 current measurements are not significantly affected by leakage. At 500 mV a 20 M Ω resistor
9 conducts 25 nA of current. Since the currents observed are much less it indicates the
10 electrochemical resistance at the graphene edge terminal is much higher and determines current
11 in the series circuit. For a 1 M KCl solution used in these measurements, the drain-source
12 conductance exhibits a squared dependence³² with pore diameter as indicated in Fig. 3c. The
13 current values for the different pore diameters also seem to be in good agreement with our
14 previous work on similar structures.²¹ For the source-gate and drain-gate measurements, the
15 graphene gate is always connected to ground to maintain a positive voltage with respect to
16 source or drain and ensure minimal leakage in accordance to our leakage measurements as
17 described earlier. This is indicated in the I-V curves for a 5 nm pore showed in Fig. 3b (and
18 Supplementary Fig. 2). The drain-gate and source-gate conductance is also plotted in Fig. 3c and
19 is observed to be nearly identical for each of the four different pores diameters, indicating that
20 the measured current is indeed only through the electrochemical exchange at the graphene
21 terminal and the leakage contribution to these measurements on the drain side is indeed
22 negligible. The o-rings used in these experiments are approximately 1.42 ± 0.1 mm in diameter.
23 Based on the leakage measurements, for a 24 nm thick Al₂O₃ insulation layer, the maximum

1 contribution of leakage at drain/source at potential of -500 mV should be approximately 30 pA,
 2 which is about two orders of magnitude less than the currents observed in these measurements.
 3 This is further confirmed by similar measurements in the same structure without a nanopore as
 4 currents in the range of 10 to 20 pA are observed across all three terminals. Furthermore, the
 5 conductance through the graphene terminal scales fairly linearly with pore diameter as seen in
 6 Fig. 3c. The slight variation from the linear dependence can be explained from the varying
 7 graphene sheet thickness (Fig. 1b) over the membrane, which affects pore sidewall area, since
 8 the pore region could consist of a mixture of mono and bi-layer graphene. Nonetheless, we do
 9 see an increase of conductance from 5 to 15 nS as the pore diameter is increased from 5 to 20
 10 nm. This is expected and indeed proves that this current is due to electrochemical exchange on
 11 the cylindrical pore sidewalls.



12
 13 Figure 3. Electrochemical measurements for embedded graphene nanoelectrode. (a) Schematic
 14 diagram of measurement setup. For the drain-source measurement (gray), source is connected to
 15 ground and voltage applied at the drain. For drain-gate (red) and drain-source (blue)
 16 measurements, the gate is connected to ground and voltage is applied to the other terminal. (b)
 17 Current-voltage curve of nanopore ionic current and electrochemical behavior of graphene edge
 18 through 5 nm nanopore. Identical currents through the drain-gate and source-gate pathways

1 indicate electrochemical exchange at the exposed graphene edge. (c) Conductance dependence
2 on pore diameter. Drain-source conductance shows a square dependence on pore diameter, while
3 gate current exchange shows a fairly linear dependence on pore diameter consistent with
4 electrochemical exchange at cylindrical nanopore wall. The slight variation from linear
5 dependence is may be attributed to varying graphene sheet thickness on various regions of the
6 membrane. 5, 9, 14 and 20 nm diameter nanopores were used in this study. All experiments are
7 performed in 1 M KCl, 10 mM Tris, 1 mM EDTA at pH 7.6

8
9 From the current values of electrochemical exchange at the 5nm pore edge, (Fig. 3b) and
10 assuming a predominantly monolayer coverage of graphene, we calculate a current density of up
11 to 1.2×10^4 A/cm² at a drain voltage of -200mV. This current density is three orders of
12 magnitude higher than electrochemical current densities reported for oxygen reduction on CNT
13 electrodes.²⁹ From electrochemistry studies on basal planes of individual monolayer sheets for
14 CVD-grown graphene reported by Li *et al.*,³³ a current density of about 6×10^{-8} A/cm² is
15 obtained. Thus a significant electrochemical current enhancement is observed using individual
16 graphene edges as the active electrode material. Furthermore, we simulated the concentration of
17 H⁺ and Cl⁻ ions at the nanopore (details in the Methods section) and the Cl⁻ ions are significantly
18 higher in number. Thus, all redox couples based on H⁺/OH⁻ ions can safely be ignored as it is
19 highly unlikely they can contribute to such high currents. Thus, we conclude that the reaction at
20 the positive graphene electrode (anode) edge is the oxidation of Cl⁻ ions. The equilibrium
21 oxidation potential for this reaction at room temperature is -1.36 V.³⁴ However surface
22 treatments enhancing the number of possible adsorption sites in diamond electrodes have been
23 reported to lower the potential of chloride oxidation by as much as 0.5 V.³⁵ A similar mechanism

1 might explain high electron transfer rates observed on graphene edges at low voltages.
2 Electrochemical studies on graphite edges have exhibited extremely high electrochemical
3 reaction rates.¹²⁻¹³ Fast electron transfer kinetics reported on CNTs are also attributed to tube
4 ends, identified as the reactive sites.^{9,36-37} For GEENs we expect all sites at the nanopore edge to
5 be damaged. Girit *et al.*¹⁷ reported TEM drilled graphene nanopores which reconstruct and
6 eventually exhibit a zigzag edge configuration due to its higher stability. For a graphene
7 nanoribbon with zigzag edges, a large peak in the density of states is observed at the edges,³⁸⁻³⁹
8 as confirmed by Scanning tunnelling microscopy (STM) studies.⁴⁰ An enhancement in the
9 density of states at the graphene nanopore edges of our architecture may have a direct effect in
10 enabling the high electrochemical current densities observed in our measurements.

11 We note an electrochemical reaction consists of mass transport of the reactive species to the
12 electrode surface and electron exchange at the electrode surface.⁴¹ Since the dominant
13 electrochemical exchange in our measurements occurs at the damaged graphene nanopore edges,
14 it would appear that the electron exchange is not the rate limiting step. Diffusion limited
15 electrochemical systems operate in the linear diffusion regime. For linear diffusion based
16 systems, *i.e.* when the electro-active length is \approx comparable to the diffusion layer thickness, the
17 reaction is diffusion limited and the peak current i_p is given by the Randles-Sevcik equation:⁹

$$i_p = 2.69 \times 10^5 n^{\frac{3}{2}} A C D^{\frac{1}{2}} \nu^{\frac{1}{2}} \quad (1)$$

18 where, n is the number of moles of electrons transferred in the reaction, A is the area of the
19 electrode (cm^2), C is the analyte concentration (in moles/ cm^3), D is the diffusion coefficient
20 (cm^2/s), and ν is the scan rate (V/s) of the applied potential. For a chloride ion oxidation
21 reaction n is assumed to be 1. The active area of the electrode is the cylindrical pore area, which
22

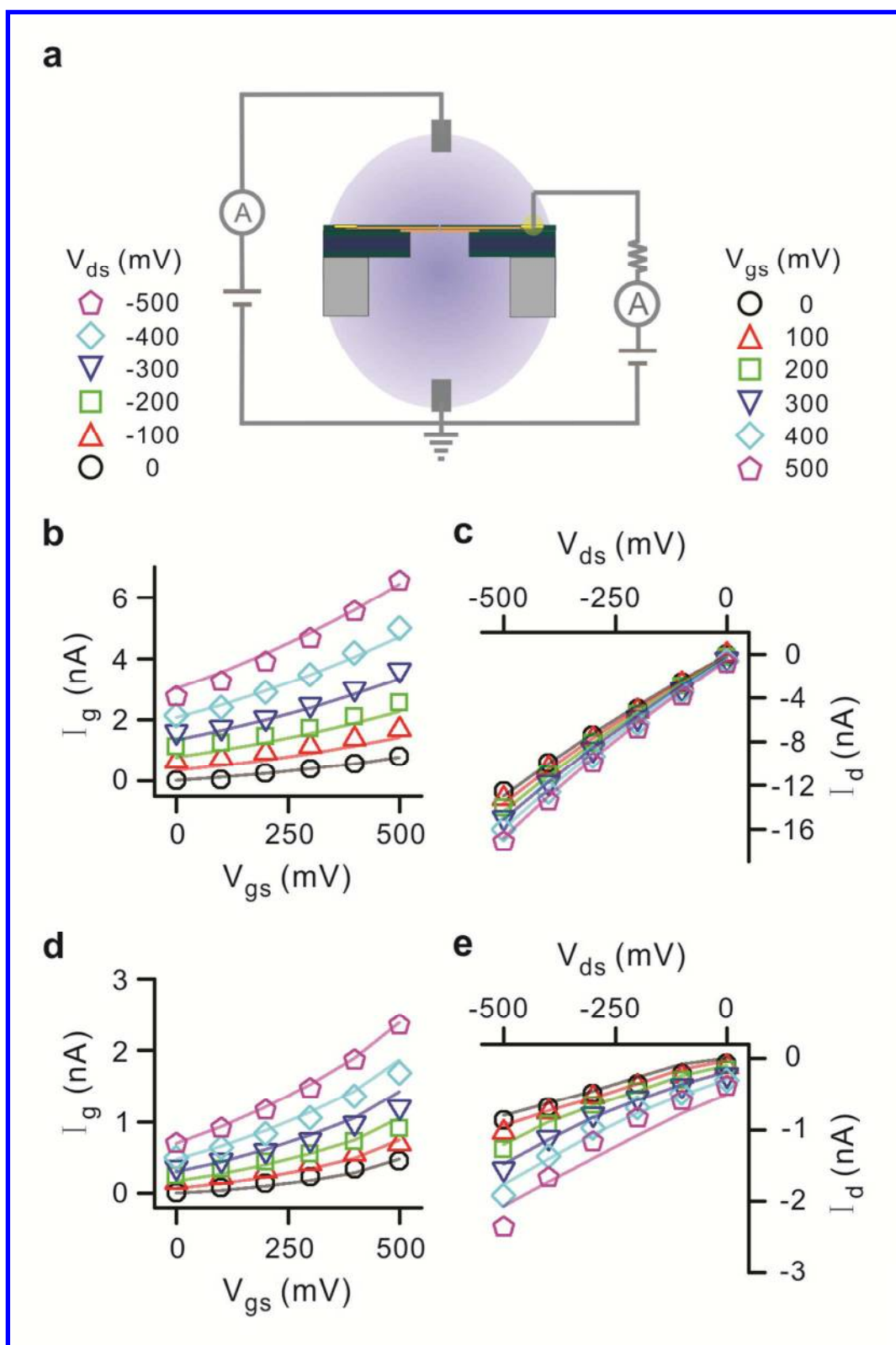
1 for a 5 nm pore, is calculated to be $9.4 \times 10^{-14} \text{ cm}^2$. The concentration is taken as 10^{-3} mol/cm^3
2 and the diffusion coefficient of Cl^- is taken as $1.5 \times 10^{-5} \text{ cm}^2/\text{s}$.⁴² For a 5nm pore and a scan rate
3 of 100 mV/10 s the peak current by the above equation gives $i_p = 9.6 \times 10^{-7} \text{ nA}$, which is much
4 smaller than observed current. Thus the reaction is not diffusion limited. It should be noted that
5 our electrode size is in nanometers and is much smaller than the diffusion layer thickness
6 (usually of the order of $\sqrt{Dt} = 3.8 \times 10^{-2} \text{ cm}$,⁴³ where t is the time period of each scan) and hence
7 convergent diffusion effects are significant. For microelectrodes, convergent diffusion leads to
8 significantly higher mass transport and thus higher current densities.⁹ We believe that with the
9 graphene nanoelectrodes used in our experiments, this effect would be exacerbated. Furthermore,
10 the local concentration of the electro-active species (Cl^-) is much higher and a threefold increase
11 has been reported when compared to microelectrodes of same electro-active area. This increase
12 in concentration is in the vicinity of the nanopore as compared to the bulk solution, also results in
13 faster mass transport,²⁰ contributing to the large current densities measured in our GEEN
14 structures. Our simulations report local (nanopore edge) concentration of Cl^- as high as 8.5 M for
15 bulk KCl concentration of 1 M (details in the Methods section).

16 We further investigate the use of our structure as a 3 terminal device analogous to a transistor
17 (Fig. 4a). The source terminal is always connected to ground in these measurements. The source
18 current can be obtained by Kirchhoff's law

$$I_d = I_g + I_s \quad (2)$$

19 where, I_d , I_g and I_s are the drain, gate and source currents respectively. In accordance with our
20 leakage results, the drain is always kept at a negative potential with respect to the gate for
21 minimal interference from leakage. The graphene gate current characteristics (I_g vs. V_{gs}) for a 5
22

1
2
3 1 nm pore in 1 M KCl solution are shown in Fig. 4b. A shift in the gate current values is observed
4
5
6 2 as the drain voltage is swept from 0 to -500 mV at a sweep rate of 100 mV/10 s (step function).
7
8 3 Numerical simulations are used to explain gate current characteristics (details in the Methods
9
10 4 section). The I_g dependence on V_{gs} and V_{ds} voltage is estimated by an exponential function. This
11
12 5 equation is coupled with the Poisson-Nernst-Planck equation and the Grahame equation and
13
14 6 solved simultaneously to obtain both gate and drain current values. Fig. 4c shows the I_d vs V_{gs}
15
16 7 characteristics. As expected, a shift in the I_d is seen as V_{gs} is swept. The simulation results are in
17
18 8 good agreement with the experimental data at 1 M KCl.
19
20
21
22
23
24
25
26
27
28
29
30
31
32
33
34
35
36
37
38
39
40
41
42
43
44
45
46
47
48
49
50
51
52
53
54
55
56
57
58
59
60



1
2
3 1 Figure 4. Three terminal measurement for the graphene embedded membrane. (a) Schematic
4
5 2 diagram with source connected to ground while voltage is swept at the drain and gate terminals.
6
7
8 3 (b) and (d) Gate current characteristics for 1 M KCl and 10 mM KCl respectively. The variation
9
10 4 of gate current with gate source bias as drain voltage is varied is shown. The scatter points are
11
12 5 experimental numbers while the straight lines are simulation fits. (c) and (e) Drain current
13
14 6 characteristics for 1 M KCl and 10 mM KCl solution respectively. The variation of drain current
15
16 7 with drain source bias as gate voltage is varied is recorded. Both solutions are prepared with 10
17
18 8 mM Tris and 1 mM EDTA for buffering at pH 7.6.
19
20
21
22 9

23
24 10 Further confirmation of observation of graphene edge currents is obtained by repeating these
25
26 11 measurements for three more pores of 9, 15 and 20 nm diameters (Fig. 5a). Since the measured
27
28 12 currents are due to electrochemical exchange at the pore walls, the active area is cylindrical.
29
30 13 Thus linear dependence of I_g on pore diameter is expected. We previously noted this in our two-
31
32 14 terminal measurements for currents due to electrochemical exchange at graphene electrodes (Fig.
33
34 15 3c). At 1 M KCl buffer solution the I_g values at two different V_{ds} (0 and -200 mV) are shown in
35
36 16 Fig. 5e and 5f, respectively, for V_{gs} swept between 0 to +500 mV. The simulated values (solid
37
38 17 lines) show excellent agreement with experimental data (symbols) for all four pore diameters.
39
40 18 We see a four-fold increase in the I_g value as the pore size is increased from 5 to 20 nm.
41
42
43
44
45
46
47
48
49
50
51
52
53
54
55
56
57
58
59
60

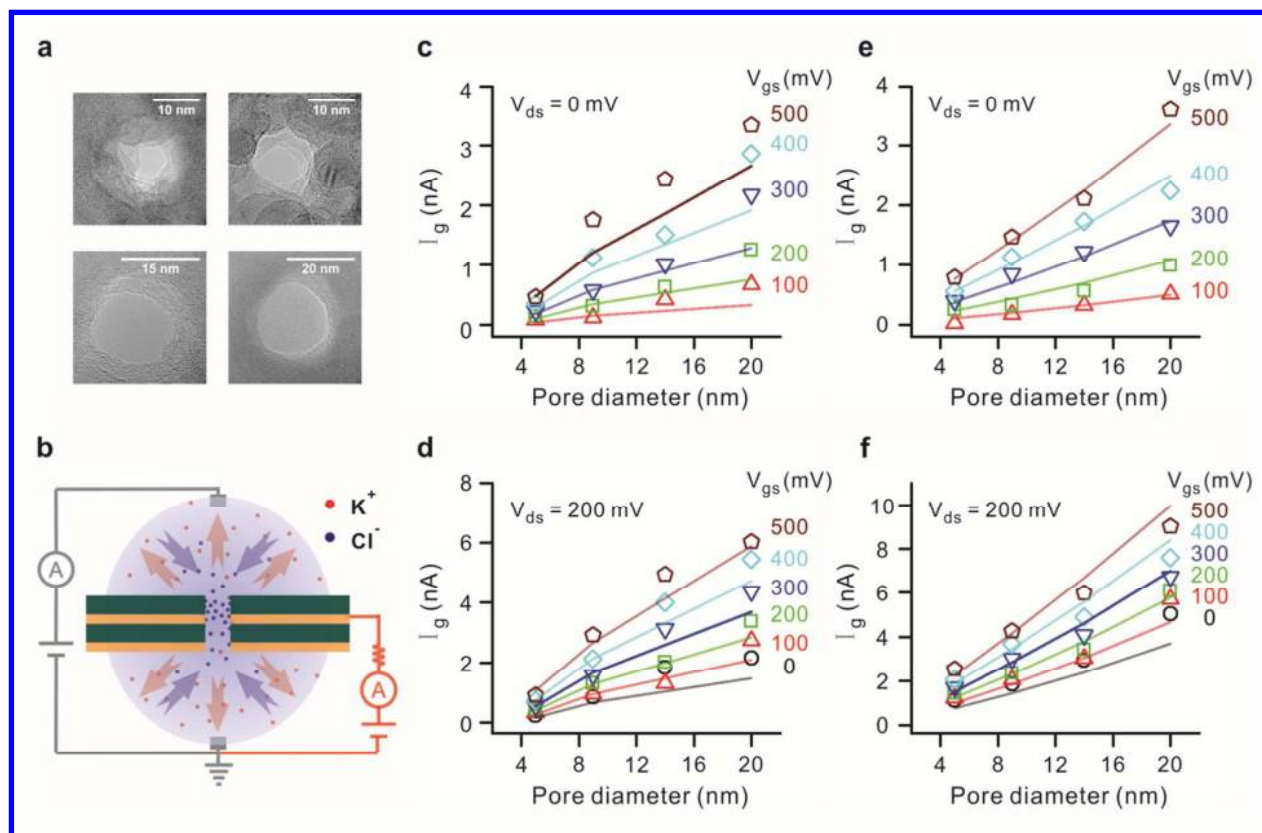


Figure 5. Gate current dependence on pore diameter (a) TEM images of nanopores of four different diameters (5, 9, 14, 20 nm) nanopores drilled through an embedded graphene membrane. (b) Schematic diagram of electrochemistry. The positive gate bias leads to attraction of chloride ions to the nanopore and expulsion of potassium ions. Red dots and arrows represent potassium ions while blue dots and arrows are for chloride ions. (c-f) Scaling of gate current with pore size at drain bias of 0 and -200 mV for 4 different pore diameters. (c), (d) Gate current dependence on pore diameter using 10 mM KCl solution. Linear dependence on pore diameter is observed over gate bias ranging from 0 to +500 mV for both drain bias values. (e), (f) Gate current dependence on pore diameter using 1 M KCl solution. Similar linear dependence on pore diameter is observed entire voltage range. The scatter points are experimental numbers while the

1
2
3 1 straight lines are simulation fits. Both solutions are prepared with 10 mM Tris and 1 mM EDTA
4
5
6 2 for buffering at pH 7.6
7

8 3
9
10 4 Similar experiments were repeated in the 10 mM KCl solution. The (I_g vs. V_{gs}) and (I_d vs. V_{ds})
11
12 5 characteristics show a similar shift as expected (Fig. 4d and 4e). The simulation results (solid
13
14 6 lines in both graphs) are in good agreement with the experimental results, although in this case
15
16 7 the fitting parameters are altered for a 5 nm pore since the pore diameter is smaller than the
17
18 8 Debye layer thickness (details in the Methods section).⁴⁴ The I_g values do not scale linearly with
19
20 9 concentration and this is attributed to enhanced ionic flux in the vicinity of the nanopore as
21
22 10 shown in our simulations (details in the Methods section). The pore diameter dependence
23
24 11 measurements in 10 mM KCl for all four pore diameters show fairly good agreement with
25
26 12 simulated results and a linear increase of I_g with pore diameter is displayed (Fig. 5c and 5d).
27
28 13 Note that the values of I_d and I_g are observed to be nearly the same for these measurements at
29
30 14 10mM, as illustrated in Supplementary Fig. 3. From equation (2), this implies an extremely low
31
32 15 I_s .
33

34
35
36
37
38 16 Our results confirm that the observation of electrochemical exchange at the graphene edge,
39
40 17 isolated from any basal plane activity. An array of GEENs could potentially be used to harness
41
42 18 extremely large value of energy density per unit mass. Methods like electron beam, nanoimprint
43
44 19 lithography or Helium based focused ion beam⁴⁵ techniques could be used to mass produce
45
46 20 arrays of nanopores. Improvement in dielectric coverage of graphene by use of other materials
47
48 21 like HfO_2 ⁴⁶ and different dielectric seed layer materials⁴⁷ like Titanium or 3,4,9,10-perylene
49
50 22 tetracarboxylic acid dianhydride (PTCDA) would significantly enhance the voltage range used in
51
52
53
54
55
56
57
58
59
60

1 these experiments by reducing parasitic leakage through the dielectric enabling higher current
2 densities to be harnessed.

3 Furthermore, we note that the differential flux in ions on opposite sides of the nanopore could
4 potentially have interesting applications in controlling the flux of bio-molecules to be sensed
5 though electrochemical exchange at the graphene edge. The differential ion flow rate could
6 potentially be used to trap molecules within the pore allowing for electrical interrogation using
7 the conductive graphene terminal. Wanunu *et al.*⁴⁸ reported the use of salt gradients as a means
8 to enhance DNA capture rate to increase throughput of the detection scheme. Another major
9 biosensing application of an embedded conductive terminal in a solid state nanopore is with
10 regards to DNA sequencing.⁴⁹ STM based studies have been demonstrated⁵⁰ to distinguish
11 deoxynucleotide monophosphates (dNMPs) and partially sequence DNA oligomers by using
12 tunnelling current measurements. Tsutsui *et al.*⁵¹⁻⁵² demonstrated tunnelling current
13 measurements to distinguish bases in deoxynucleotide triphosphate (dNTP) molecules. If an
14 embedded conductive terminal, *e.g.* GEENs, can be combined with biological⁵³ or electronic⁵⁴
15 methods to slow DNA translocation rates, it could provide a pathway to DNA sequencing.

16 **Conclusion**

17 In summary, we present the investigation of electrochemical current exchange at a CVD-grown
18 graphene edges within a nanopore. We demonstrate the ability of our graphene embedded
19 nanopore structures to study electrochemistry at individual graphene layers in isolation from
20 contribution from basal planes. We observed electrochemical current densities on the order of
21 10^4 A/cm², three orders of magnitude higher than those reported for carbon nanotubes and much
22 higher than those reported for graphene surface electrochemical studies. The high currents are
23 attributed to a combination of the nanopore edge structures produced by electron beam sculpting

1 along with the convergent diffusion mechanisms due to nanosized electrodes, which have been
2 reported to enhance ionic flux of reactive species. We also demonstrated the modulation of ionic
3 current by the use of the embedded conductive graphene terminal. Numerical simulations were
4 performed to confirm the transistor like characteristics of the device. Extremely high
5 electrochemical current densities have exciting applications for both chemical and biological
6 sensing as well as energy storage. Scaling of these structures by producing arrays of nanopores
7 could enable multiple applications.

8 **Experimental Details**

9 **Graphene Growth and Transfer:**

10 Graphene is grown by chemical vapor deposition (CVD) on 1.4 mil copper foils purchased from
11 Basic Copper.^{21,24,55} Copper foil is placed in an Atomate CVD system and annealed at ~1000 °C
12 under Ar/H₂ flow for 90 minutes at a base pressure of ≈ 4.4 Torr. Graphene is grown for 30
13 minutes at 1000 °C under 850 sccm of CH₄ and 50 sccm of H₂ at a base pressure of about 2.5
14 Torr. The resulting graphene and Cu substrates are cooled to 400 °C under 850 sccm of CH₄, 50
15 sccm of H₂ at a rate of ~ 10 °C/minute followed by cooling to room temperature under 500 sccm
16 of Ar while the base pressure is ramped to 760 Torr (Supplementary Fig. 8a). Graphene is
17 transferred to the receiving substrates by coating one side of the Cu foil with a bilayer of PMMA
18 (495 K A2 and 950 K A4) (Supplementary Fig. 8b-i). Each layer of PMMA is coated at 3000
19 rpm followed by a 200 °C bake for 2 min. The backside graphene is removed by O₂ plasma
20 etching prior to etching the Cu foil (Supplementary Fig. 8b-ii) in etchant overnight (Transcene
21 CE-100). The resultant PMMA/graphene film is transferred to a 10% HCl in deionized (DI)
22 water solution to remove residual metal particles followed by a second DI rinse (Supplementary
23 Fig. 8b-iii). The film is then transferred onto the receiving substrate (Supplementary Fig. 8b-iv)

1 with predefined FIB holes (~ 300 nm in diameter) and PMMA is removed in a 1:1 methylene
2 chloride/methanol solution for 30 min. The samples undergo a 400 °C anneal under Ar (500
3 sccm) and H₂ (100 sccm) flow to remove residual PMMA.

4 **Raman Spectroscopy and AFM Characterization:**

5 Raman mapping is performed using a scanning confocal Renishaw Raman microscope (inVia and
6 WiRE 3.2 software). Data is collected using a 633 nm edge emitting laser (laser spot size ~ 1.3
7 μm and ~ 0.1 mW incident power), a 50 \times long working distance objective, a 1800 lines/mm
8 grating, and 30 s acquisition time. 121 spectra is collected over $20 \times 20 \mu\text{m}^2$ area at a 2 μm step
9 size and analyzed by fitting mixed Gaussian and Lorentzian curves around the D, G, and 2D
10 Raman peaks centered at ≈ 1340 , 1590, and 2660 cm^{-1} , respectively. A cubic spline interpolation
11 is used to subtract the background before curve fitting. Atomic force microscope (AFM) data is
12 collected using a Digital Instruments Dimension 3000 AFM in a tapping mode. Calculated root-
13 mean-square (RMS) roughness values are obtained using Nanoscope Analysis v.1.4 software
14 from Bruker Corporation. Three dimensional images are rendered using Gwyddion AFM
15 analysis software.

16 **Supporting Membranes:**

17 Membranes consisting of stacked layers of Al₂O₃ and SiN_x is fabricated on $300 \pm 2 \mu\text{m}$ thick
18 double-side polished <100> silicon wafers purchased from Silicon Quest International. Wafers
19 are piranha cleaned (1:1 H₂SO₄:H₂O₂) for 15 minutes before depositing Al₂O₃ *via* ALD
20 (Cambridge Nanotech). 50 nm of Al₂O₃ was deposited at a platen temperature of 250 °C using
21 tetramethyl-aluminum (TMA) and water vapor precursors. Subsequently, 200 nm of low-stress
22 SiN_x is deposited (STS Mesc PECVD System) using a mixed-frequency recipe (High Frequency:
23 6 s at 13.56 MHz, platen power of 20 W and Low Frequency: 2 s at 380 kHz, platen power of 60

1
2
3 1 W) with precursors SiH_4 and NH_3 at flow rates of 40 sccm and 55 sccm, respectively, at a platen
4
5 2 temperature of 300 °C. Another 50 nm of Al_2O_3 (ALD) is deposited with the same parameters as
6
7 3 described before. Optical lithography is used to define 80 μm square windows on the back of the
8
9 4 wafer with the aid of plasma resistant Megaposit SPR-220 photoresist and an ABM Flood
10
11 5 Exposure (Model 60) tool. The wafer is then placed inside a STS Pegasus ICP DRIE and 80 μm
12
13 6 square membranes are suspended using a Bosch etching process. 300 to 350 nm holes are then
14
15 7 formed in these membranes using a focused ion beam (FIB) (FEI DB235) operated at a beam
16
17 8 current of 30 pA.
18
19
20
21

22 9 **Nanopore Fabrication and Nanopore Fluidic Measurement**

23
24 10 The graphene- Al_2O_3 -graphene- Al_2O_3 stack is fabricated sequentially using the same graphene
25
26 11 transfer and ALD process as described previously. The thickness of Al_2O_3 for both dielectric
27
28 12 layers is 24 nm. A seed layer Al (2nm thick) is deposited on graphene using a CHA SEC-600
29
30 13 electron-beam evaporator prior to deposition of both dielectric layers. The second (top) graphene
31
32 14 layer is contacted with Ti/Au contacts. Electrical contacts, Ti (2 nm thickness adhesion layer)
33
34 15 and Au (300 nm thick), are deposited onto G2 by shadow masking and e-beam evaporation. The
35
36 16 measured sheet resistance of graphene is 6.7 $\text{k}\Omega/\square$. Single nanopores of 5-20 nm diameter are
37
38 17 drilled in the graphene-embedded membrane using a JOEL 2010F field-emission gun TEM
39
40 18 operated at 200 kV in CBED mode with focused electron probe of diameter = 1.6 nm. O_2 plasma
41
42 19 treatment at 50 W for 30 sec on source side facilitates wetting. Subsequently Al wires are
43
44 20 attached on Ti/Au contacts using silver paint and the chip is assembled in a custom-built
45
46 21 chamber. Ethanol is filled in both reservoirs initially to promote wetting. Subsequently the
47
48 22 ethanol is flushed out and the reservoirs are filled with a solution of 1 M KCl, 10 mM Tris, 1
49
50
51
52
53
54
55
56
57
58
59
60

1 mM EDTA at pH 7.6. All nanopore experiments are performed with Axopatch 200B and Digidata 1440A at room temperature (22 ± 2 °C).

3 Electrostatic Simulations

4 The mathematical model for ion transport involves a set of equations governing ionic transport and the electric potential.⁵⁶

6 The total flux due to diffusion and electromigration of the *ith* species (ions) is given by the following expression

$$\mathbf{\Gamma}_i = -D_i \nabla c_i - \frac{D_i}{RT} z_i F c_i \nabla \phi \quad (3)$$

9 where F is the Faraday's constant, z_i is the valence, D_i is the diffusion coefficient, $\mathbf{\Gamma}_i$ is the flux, c_i is the concentration of the *ith* species, and ϕ is the electrical potential. The Nernst-Planck (NP) equation describes the reaction rate (r_i) of dissolved species.

$$\frac{\partial c_i}{\partial t} = -\nabla \cdot \mathbf{\Gamma}_i + r_i \quad (4)$$

13 The electrical potential distribution is governed by the Poisson equation

$$\nabla \cdot (\epsilon_r \nabla \phi) = -\frac{F \sum z_i c_i}{\epsilon_0} \quad (5)$$

15 where ϵ_0 is the permittivity of vacuum and ϵ_r is the relative permittivity. The electric potential at the wall surface is governed by

$$\frac{\partial \phi}{\partial n} = -\frac{\sigma_s}{\epsilon_0 \epsilon_r} \quad (6)$$

18 where σ_s is the surface charge density and n is the normal to the wall.

1
2
3 1 The Poisson-Nernst-Planck equations (PNP) equations can be simplified by integrating equation
4
5
6 2 (3) and (5) across the channel, which gives

$$7 \quad \frac{\partial \bar{c}_i}{\partial t} = \frac{1}{A} \frac{\partial}{\partial x} \left(AD_i \frac{\partial \bar{c}_i}{\partial x} + A \frac{D_i}{RT} z_i F \bar{c}_i \frac{\partial \bar{\phi}}{\partial x} \right) + \bar{r}_i \quad (7)$$

8
9
10
11
12
13 4 and

$$14 \quad \frac{\partial}{\partial x} \left(A \frac{\partial \bar{\phi}}{\partial x} \right) = - \frac{A \left(F \sum z_i \bar{c}_i + 4\sigma_s / d \right)}{\epsilon_r \epsilon_0} \quad (8)$$

15
16
17
18
19
20
21
22 6
23
24 7 where A is the cross-sectional area, x is the coordinate along the channel, d is the nanopore
25
26
27 8 diameter, \bar{c}_i , \bar{r}_i , $\bar{\phi}$ are the cross-sectional averaged concentration, reaction rate, and electric
28
29
30 9 potential, respectively.

31
32
33 10 From equation (7) and (8), we obtain the cross-sectional averaged electric potential, and ionic
34
35 11 concentration. The drain current is calculated by multiplying the current density along the x
36
37 12 direction (assumed normal to pore wall) with the cross-sectional area at drain.

$$38 \quad I_x = \sum_i z_i F \Gamma_{xi} \quad (9)$$

39
40
41
42
43
44 14 where Γ_{xi} is the flux rate of i th species in the x direction.

45
46
47 15 The gate current is calculated from the reaction rate of the species near the graphene gate. The
48
49 16 oxidation rate of Cl^- is assumed as a function of the electrical potential bias and the local
50
51 17 concentration.

$$52 \quad \bar{r}_{\text{Cl}^-} = -r_{0\text{Cl}^-} \left[\exp(aV_G - bV_D) - 1 \right] \bar{c}_{\text{Cl}^-} \quad (10)$$

1 where r_{0Cl^-} , a and b are fitting parameters. \bar{c}_{Cl^-} is the cross-sectional averaged concentration of
 2 Cl^- at pore surface (mM or mole/m³).

3 Near the graphene gate edge, water oxidation, which generated H^+ ions.



5 The generation rate of H^+ is assumed as

$$6 \quad \bar{r}_{H^+} = -r_{0H^+} [\exp(aV_G - bV_D) - 1] \quad (12)$$

7 The gate current I_G is calculated from

$$8 \quad I_G = \frac{\pi}{4} d^2 l_r F (\bar{r}_{H^+} - \bar{r}_{Cl^-}) \quad (13)$$

9 where l_r is the length of reaction region. In the simulations, l_r is taken as 2nm, $r_{0Cl^-} = 5 \times 10^7 \text{ s}^{-1}$,
 10 and $r_{0H^+} = 2 \times 10^7 \text{ mol/m}^3/\text{s}$. The parameters a and b are correlated to the pore size and
 11 electrolyte concentrations. In these simulations, $d > \kappa^{-1}$ where κ^{-1} is the debye layer thickness, we
 12 choose $a = 0.66 \text{ V}^{-1}$, and $b = 2.05 \text{ V}^{-1}$. However when $d < \kappa^{-1}$, for $d = 5\text{nm}$ and KCl concentration
 13 of 10 mM, we choose $a = 0.625 \text{ V}^{-1}$, and $b = 1.25 \text{ V}^{-1}$. The gate current from water oxidation is
 14 much smaller than that from Cl^- oxidation. However water oxidation induces H^+ ions in the
 15 nanopore, which affects the surface charge density of the Al_2O_3 layer.

16 The surface charge density of the Al_2O_3 layer is determined by the density difference of the sites
 17 attracting positive and negative charges.

$$18 \quad \sigma_s = e(N_+ - N_-) \quad (14)$$

$$19 \quad N = N_+ + N_- + N_0 \quad (15)$$

1 where N_+ , N_- , and N_0 are the density of positively charged, negatively charged, and neutral sites,
 2 respectively.

3 The densities of the positively and negatively charged sites are related to the pH value and
 4 surface potential ψ_s .⁵⁷

$$\frac{N_+ N_0^{ISP}}{N_+^{ISP} N_0} = \frac{\bar{c}_{H^+}}{c_{H^+}^{ISP}} \exp\left(-\frac{F\psi_s}{RT}\right) \quad (16)$$

$$\frac{N_- N_0^{ISP}}{N_-^{ISP} N_0} = \frac{c_{H^+}^{ISP}}{\bar{c}_{H^+}} \exp\left(\frac{F\psi_s}{RT}\right) \quad (17)$$

7 where ISP is the isoelectric point, c_{H^+} is the H^+ concentration in the nanopore. The surface
 8 charge density is obtained by the Grahame equation.³⁴

$$\sigma_s = \epsilon_r \epsilon_0 \frac{RT}{zF} \kappa \sinh\left(\frac{F\psi_s}{2RT}\right) \quad (18)$$

10 Given N , $c_{H^+}^{ISP}$, and N_0^{ISP} , the surface charge density can be obtained by solving equations
 11 (14)-(18). In the simulations, $c_{H^+}^{ISP}$ is chosen as 10^{-8} mM, $N = 6$ /nm², and $N_0^{ISP} = 2$ /nm². We
 12 calculate $\bar{c}_{H^+} = 0.01$ mM in a 5 nm pore (for $V_{ds} = -500$ mV and $V_{gs} = 500$ mV). We also
 13 calculate $\bar{c}_{Cl^-} = 5000$ mM and $\bar{c}_{Cl^-} = 8500$ mM for 10mM and 1000mM KCl solutions
 14 respectively.

15 Acknowledgements

16 The authors would like to acknowledge support from the National Institutes of Health (R21
 17 CA155863) and Oxford Nanopore Technologies, U.K for supporting the effort. D. Estrada and E.

1 Pop acknowledge support from the National Science Foundation (NSF) Graduate Research
2 Fellowship Program and CAREER award ECCS 09-54423, respectively.

3 **Supporting Information**

4 Leakage studies, additional graphene electrochemical studies, photographs of experimental
5 setup, characterization of graphene transfer process and dielectric deposition. This material is
6 available free of charge *via* the Internet at <http://pubs.acs.org>

7 **References**

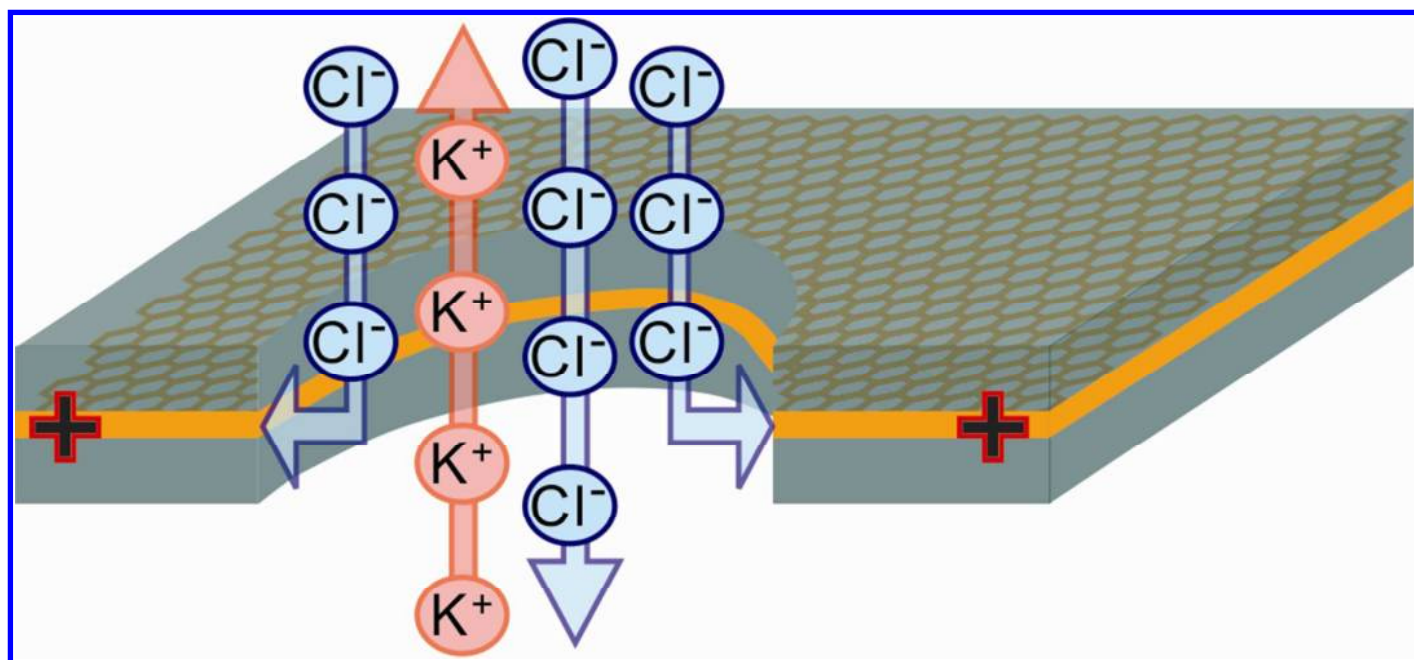
- 8 1. Novoselov, K. S.; Geim, A. K.; Morozov, S. V.; Jiang, D.; Zhang, Y.; Dubonos, S. V.;
9 Grigorieva, I. V.; Firsov, A. A., Electric Field Effect in Atomically Thin Carbon Films. *Science* **2004**,
10 *306*, 666-669.
- 11 2. Bolotin, K. I.; Sikes, K. J.; Jiang, Z.; Klima, M.; Fudenberg, G.; Hone, J.; Kim, P.; Stormer, H.
12 L., Ultrahigh Electron Mobility in Suspended Graphene. *Solid State Commun.* **2008**, *146*, 351-
13 355.
- 14 3. Balandin, A. A., Thermal Properties of Graphene and Nanostructured Carbon Materials.
15 *Nat. Mater.* **2011**, *10*, 569-581.
- 16 4. Mak, K. F.; Shan, J.; Heinz, T. F., Electronic Structure of Few-Layer Graphene:
17 Experimental Demonstration of Strong Dependence on Stacking Sequence. *Phys. Rev. Lett.*
18 **2010**, *104*, 176404.
- 19 5. Pumera, M., Electrochemistry of Graphene: New Horizons for Sensing and Energy
20 Storage. *Chem. Rec.* **2009**, *9*, 211-223.
- 21 6. Hou, J.; Shao, Y.; Ellis, M. W.; Moore, R. B.; Yi, B., Graphene-Based Electrochemical
22 Energy Conversion and Storage: Fuel Cells, Supercapacitors and Lithium Ion Batteries. *Phys.*
23 *Chem. Chem. Phys.* **2011**, *13*, 15384-15402.
- 24 7. Shao, Y.; Wang, J.; Wu, H.; Liu, J.; Aksay, I. A.; Lin, Y., Graphene Based Electrochemical
25 Sensors and Biosensors: A Review. *Electroanalysis* **2010**, *22*, 1027-1036.
- 26 8. Brownson, D. A.; Banks, C. E., Graphene Electrochemistry: An Overview of Potential
27 Applications. *The Analyst* **2010**, *135*, 2768-2778.
- 28 9. Banks, C. E.; Davies, T. J.; Wildgoose, G. G.; Compton, R. G., Electrocatalysis at Graphite
29 and Carbon Nanotube Modified Electrodes: Edge-Plane Sites and Tube Ends Are the Reactive
30 Sites. *Chem. Commun. (Cambridge, U.K.)* **2005**, 829-841.
- 31 10. Durkan, C.; Welland, M. E., Analysis of Failure Mechanisms in Electrically Stressed Gold
32 Nanowires. *Ultramicroscopy* **2000**, *82*, 125-133.
- 33 11. Behnam, A.; Lyons, A. S.; Bae, M.-H.; Chow, E. K.; Islam, S.; Neumann, C. M.; Pop, E.,
34 Transport in Nanoribbon Interconnects Obtained from Graphene Grown by Chemical Vapor
35 Deposition. *Nano Lett.* **2012**, *12*, 4424-4430.

- 1
2
3
4
5
6
7
8
9
10
11
12
13
14
15
16
17
18
19
20
21
22
23
24
25
26
27
28
29
30
31
32
33
34
35
36
37
38
39
40
41
42
43
44
45
46
47
48
49
50
51
52
53
54
55
56
57
58
59
60
12. Ambrosi, A.; Bonanni, A.; Pumera, M., Electrochemistry of Folded Graphene Edges. *Nanoscale* **2011**, *3*, 2256-2260.
 13. Davies, T. J.; Hyde, M. E.; Compton, R. G., Nanotrench Arrays Reveal Insight into Graphite Electrochemistry. *Angew. Chem., Int. Ed. Engl.* **2005**, *44*, 5121-5126.
 14. Zhou, M.; Zhai, Y.; Dong, S., Electrochemical Sensing and Biosensing Platform Based on Chemically Reduced Graphene Oxide. *J. Anal. Chem.* **2009**, *81*, 5603-5613.
 15. Liu, C.; Yu, Z.; Neff, D.; Zhamu, A.; Jang, B. Z., Graphene-Based Supercapacitor with an Ultrahigh Energy Density. *Nano Lett.* **2010**, *10*, 4863-4868.
 16. Yoo, J. J.; Balakrishnan, K.; Huang, J.; Meunier, V.; Sumpter, B. G.; Srivastava, A.; Conway, M.; Reddy, A. L.; Yu, J.; Vajtai, R., *et al.*, Ultrathin Planar Graphene Supercapacitors. *Nano Lett.* **2011**, *11*, 1423-1427.
 17. Girit, Ç. Ö.; Meyer, J. C.; Erni, R.; Rossell, M. D.; Kisielowski, C.; Yang, L.; Park, C.-H.; Crommie, M. F.; Cohen, M. L.; Louie, S. G., *et al.*, Graphene at the Edge: Stability and Dynamics. *Science* **2009**, *323*, 1705-1708.
 18. Merchant, C. A.; Healy, K.; Wanunu, M.; Ray, V.; Peterman, N.; Bartel, J.; Fischbein, M. D.; Venta, K.; Luo, Z.; Johnson, A. T., *et al.*, DNA Translocation through Graphene Nanopores. *Nano Lett.* **2010**, *10*, 2915-2921.
 19. Schneider, G. F.; Kowalczyk, S. W.; Calado, V. E.; Pandraud, G.; Zandbergen, H. W.; Vandersypen, L. M.; Dekker, C., DNA Translocation through Graphene Nanopores. *Nano Lett.* **2010**, *10*, 3163-3167.
 20. Zhang, Y.; Zhang, B.; White, H. S., Electrochemistry of Nanopore Electrodes in Low Ionic Strength Solutions. *J. Phys. Chem. B* **2006**, *110*, 1768-1774.
 21. Venkatesan, B. M.; Estrada, D.; Banerjee, S.; Jin, X.; Dorgan, V. E.; Bae, M.-H.; Aluru, N. R.; Pop, E.; Bashir, R., Stacked Graphene-Al₂O₃ Nanopore Sensors for Sensitive Detection of DNA and DNA-Protein Complexes. *ACS Nano* **2011**, *6*, 441-450.
 22. Liang, X.; Sperling, B. A.; Calizo, I.; Cheng, G.; Hacker, C. A.; Zhang, Q.; Obeng, Y.; Yan, K.; Peng, H.; Li, Q., *et al.*, Toward Clean and Crackless Transfer of Graphene. *ACS Nano* **2011**, *5*, 9144-9153.
 23. Lenski, D. R.; Fuhrer, M. S., Raman and Optical Characterization of Multilayer Turbostratic Graphene Grown *Via* Chemical Vapor Deposition. *J. Appl. Phys.* **2011**, *110*.
 24. Salehi-Khojin, A.; Estrada, D.; Lin, K. Y.; Bae, M.-H.; Xiong, F.; Pop, E.; Masel, R. I., Polycrystalline Graphene Ribbons as Chemiresistors. *Adv. Mater.* **2012**, *24*, 53-57.
 25. Kim, S.; Nah, J.; Jo, I.; Shahrjerdi, D.; Colombo, L.; Yao, Z.; Tutuc, E.; Banerjee, S. K., Realization of a High Mobility Dual-Gated Graphene Field-Effect Transistor with Al₂O₃ Dielectric. *Appl. Phys. Lett.* **2009**, *94*, 062107.
 26. Wang, L.; Travis, J. J.; Cavanagh, A. S.; Liu, X.; Koenig, S. P.; Huang, P. Y.; George, S. M.; Bunch, J. S., Ultrathin Oxide Films by Atomic Layer Deposition on Graphene. *Nano Lett.* **2012**, *12*, 3706-3710.
 27. Venkatesan, B. M.; Dorvel, B.; Yemenicioglu, S.; Watkins, N.; Petrov, I.; Bashir, R., Highly Sensitive, Mechanically Stable Nanopore Sensors for DNA Analysis. *Adv. Mater.* **2009**, *21*, 2771-2776.

- 1
2
3
4
5
6
7
8
9
10
11
12
13
14
15
16
17
18
19
20
21
22
23
24
25
26
27
28
29
30
31
32
33
34
35
36
37
38
39
40
41
42
43
44
45
46
47
48
49
50
51
52
53
54
55
56
57
58
59
60
- 1 28. Chen, P.; Mitsui, T.; Farmer, D. B.; Golovchenko, J.; Gordon, R. G.; Branton, D., Atomic
2 Layer Deposition to Fine-Tune the Surface Properties and Diameters of Fabricated Nanopores.
3 *Nano Lett.* **2004**, *4*, 1333-1337.
- 4 29. Paik, K. H.; Liu, Y.; Tabard-Cossa, V.; Waugh, M. J.; Huber, D. E.; Provine, J.; Howe, R. T.;
5 Dutton, R. W.; Davis, R. W., Control of DNA Capture by Nanofluidic Transistors. *ACS Nano* **2012**,
6 *6*, 6767-6775.
- 7 30. Reddy, B., Jr.; Dorvel, B.; Go, J.; Nair, P.; Elibol, O.; Credo, G.; Daniels, J.; Chow, E. C.; Su,
8 X.; Varma, M., *et al.*, High-K Dielectric Al₂O₃ Nanowire and Nanoplate Field Effect Sensors for
9 Improved Ph Sensing. *Biomed. Microdevices* **2011**, *13*, 335-344.
- 10 31. Wallrapp, F.; Fromherz, P., TiO₂ and HfO₂ in Electrolyte-Oxide-Silicon Configuration for
11 Applications in Bioelectronics. *J. Appl. Phys.* **2006**, *99*, 114103.
- 12 32. Smeets, R. M. M.; Keyser, U. F.; Krapf, D.; Wu, M.-Y.; Dekker, N. H.; Dekker, C., Salt
13 Dependence of Ion Transport and DNA Translocation through Solid-State Nanopores. *Nano Lett.*
14 **2005**, *6*, 89-95.
- 15 33. Li, W.; Tan, C.; Lowe, M. A.; Abruña, H. c. D.; Ralph, D. C., Electrochemistry of Individual
16 Monolayer Graphene Sheets. *ACS Nano* **2011**, *5*, 2264-2270.
- 17 34. Bard, A. J.; Faulkner, L. R., *Electrochemical Methods : Fundamentals and Applications*.
18 2nd ed.; Wiley: New York, 2001; pp 124,546,808.
- 19 35. McCreery, R. L., Advanced Carbon Electrode Materials for Molecular Electrochemistry.
20 *Chem. Rev.* **2008**, *108*, 2646-2687.
- 21 36. Britto, P. J.; Santhanam, K. S. V.; Rubio, A.; Alonso, J. A.; Ajayan, P. M., Improved Charge
22 Transfer at Carbon Nanotube Electrodes. *Adv. Mater.* **1999**, *11*, 154-157.
- 23 37. Nugent, J. M.; Santhanam, K. S. V.; Rubio, A.; Ajayan, P. M., Fast Electron Transfer
24 Kinetics on Multiwalled Carbon Nanotube Microbundle Electrodes. *Nano Lett.* **2001**, *1*, 87-91.
- 25 38. Krauss, B.; Nemes-Incze, P.; Skakalova, V.; Biro, L. P.; Klitzing, K.; Smet, J. H., Raman
26 Scattering at Pure Graphene Zigzag Edges. *Nano Lett.* **2010**, *10*, 4544-4548.
- 27 39. Saha, K. K.; Drndic, M.; Nikolic, B. K., DNA Base-Specific Modulation of Microampere
28 Transverse Edge Currents through a Metallic Graphene Nanoribbon with a Nanopore. *Nano*
29 *Lett.* **2012**, *12*, 50-55.
- 30 40. Ritter, K. A.; Lyding, J. W., The Influence of Edge Structure on the Electronic Properties
31 of Graphene Quantum Dots and Nanoribbons. *Nat. Mater.* **2009**, *8*, 235-242.
- 32 41. Rieger, P. H., *Electrochemistry*. 2nd ed.; Chapman & Hall: New York, 1994; pp 152.
- 33 42. Liu, J.; Kvetny, M.; Feng, J.; Wang, D.; Wu, B.; Brown, W.; Wang, G., Surface Charge
34 Density Determination of Single Conical Nanopores Based on Normalized Ion Current
35 Rectification. *Langmuir* **2011**, *28*, 1588-1595.
- 36 43. Bockris, J. O. M.; Reddy, A. K. N., *Modern Electrochemistry*. 2nd ed.; Plenum Press: New
37 York, 1998; pp 1234.
- 38 44. Israelachvili, J. N., *Intermolecular and Surface Forces*. 2nd ed.; Academic Press London:
39 1991; pp 238.
- 40 45. Precision Material Modification and Patterning with He Ions. *J. Vac. Sci. Technol., B:*
41 *Microelectron. Nanometer Struct.* **2009**, *27*, 2755.

- 1
2
3 1 46. Dorvel, B. R.; Reddy, B.; Go, J.; Duarte Guevara, C.; Salm, E.; Alam, M. A.; Bashir, R.,
4 2 Silicon Nanowires with High-K Hafnium Oxide Dielectrics for Sensitive Detection of Small
5 3 Nucleic Acid Oligomers. *ACS Nano* **2012**, *6*, 6150-6164.
6 4 47. Fallahazad, B.; Lee, K.; Lian, G.; Kim, S.; Corbet, C. M.; Ferrer, D. A.; Colombo, L.; Tutuc,
7 5 E., Scaling of Al₂O₃ Dielectric for Graphene Field-Effect Transistors. *Appl. Phys. Lett.* **2012**, *100*,
8 6 093112.
9 7 48. Wanunu, M.; Morrison, W.; Rabin, Y.; Grosberg, A. Y.; Meller, A., Electrostatic Focusing
10 8 of Unlabelled DNA into Nanoscale Pores Using a Salt Gradient. *Nat. Nanotechnol.* **2010**, *5*, 160-
11 9 165.
12 10 49. Venkatesan, B. M.; Bashir, R., Nanopore Sensors for Nucleic Acid Analysis. *Nat.*
13 11 *Nanotechnol.* **2011**, *6*, 615-624.
14 12 50. Huang, S.; He, J.; Chang, S.; Zhang, P.; Liang, F.; Li, S.; Tuchband, M.; Fuhrmann, A.; Ros,
15 13 R.; Lindsay, S., Identifying Single Bases in a DNA Oligomer with Electron Tunnelling. *Nat.*
16 14 *Nanotechnol.* **2010**, *5*, 868-873.
17 15 51. Tsutsui, M.; Taniguchi, M.; Yokota, K.; Kawai, T., Identifying Single Nucleotides by
18 16 Tunnelling Current. *Nat. Nanotechnol.* **2010**, *5*, 286-290.
19 17 52. Tsutsui, M.; Rahong, S.; Iizumi, Y.; Okazaki, T.; Taniguchi, M.; Kawai, T., Single-Molecule
20 18 Sensing Electrode Embedded in-Plane Nanopore. *Sci. Rep.* **2011**, *1*, 46.
21 19 53. Cherf, G. M.; Lieberman, K. R.; Rashid, H.; Lam, C. E.; Karplus, K.; Akeson, M., Automated
22 20 Forward and Reverse Ratcheting of DNA in a Nanopore at 5-Å Precision. *Nat. Biotechnol.* **2012**,
23 21 *30*, 344-348.
24 22 54. He, Y.; Tsutsui, M.; Fan, C.; Taniguchi, M.; Kawai, T., Controlling DNA Translocation
25 23 through Gate Modulation of Nanopore Wall Surface Charges. *ACS Nano* **2011**, *5*, 5509-5518.
26 24 55. Kim, R.-H.; Bae, M.-H.; Kim, D. G.; Cheng, H.; Kim, B. H.; Kim, D.-H.; Li, M.; Wu, J.; Du, F.;
27 25 Kim, H.-S., *et al.*, Stretchable, Transparent Graphene Interconnects for Arrays of Microscale
28 26 Inorganic Light Emitting Diodes on Rubber Substrates. *Nano Lett.* **2011**, *11*, 3881-3886.
29 27 56. Karniadakis, G.; Beskök, A.; Aluru, N. R., *Microflows and Nanoflows : Fundamentals and*
30 28 *Simulation*. Springer: New York, NY, 2005; pp 255-304.
31 29 57. Mustafa, S.; Dilara, B.; Neelofer, Z.; Naeem, A.; Tasleem, S., Temperature Effect on the
32 30 Surface Charge Properties of γ -Al₂O₃. *J. Colloid Interface Sci.* **1998**, *204*, 284-293.
33
34
35
36
37
38
39
40
41
42
43
44
45
46
47
48
49
50
51
52
53
54
55
56
57
58
59
60

37 **Table of content graphic**



1

2